JYX
JYVÄSKYLÄN YLIOPISTO
UNIVERSITY OF JYVÄSKYLÄ

This is a self-archived version of an original article. This version may differ from the original in pagination and typographic details.

Author(s): Bogachev, A. A.; Kozulin, E. M.; Knyazheva, G. N.; Itkis, I. M.; Itkis, M. G.; Novikov, K. V.; Kumar, D.; Banerjee, T.; Diatlov, I. N.; Cheralu, M.; Kirakosyan, V. V.; Mukhamejanov, Y. S.; Pan, A. N.; Pchelintsev, I. V.; Tikhomirov, R. S.; Vorobiev, I. V.; Maiti, M.; Prajapat, R.; Kumar, R.; Sarkar, G.; Trzaska, W. H.; Andreyev, A. N.; Harca, I. M.; Vardaci, E.

Title: Asymmetric and symmetric fission of excited nuclei of 180,190Hg and 184,192,202Pb formed in the reactions with 36Ar and 40,48Ca ions

Year: 2021

Version: Published version

Copyright: ©2021 American Physical Society

Rights: In Copyright

Rights url: http://rightsstatements.org/page/InC/1.0/?language=en

Please cite the original version:

Bogachev, A.A., Kozulin, E. M., Knyazheva, G. N., Itkis, I. M., Itkis, M. G., Novikov, K. V., Kumar, D., Banerjee, T., Diatlov, I. N., Cheralu, M., Kirakosyan, V.V., Mukhamejanov, Y. S., Pan, A. N., Pchelintsev, I. V., Tikhomirov, R. S., Vorobiev, I. V., Maiti, M., Prajapat, R., Kumar, R., . . . Vardaci, E. (2021). Asymmetric and symmetric fission of excited nuclei of 180,190Hg and 184,192,202Pb formed in the reactions with 36Ar and 40,48Ca ions. Physical Review C, 104(2), Article 024623. https://doi.org/10.1103/PhysRevC.104.024623

Asymmetric and symmetric fission of excited nuclei of ^{180,190}Hg and ^{184,192,202}Pb formed in the reactions with ^{36}Ar and ^{40,48}Ca ions

A. A. Bogachev,[1] E. M. Kozulin,[1] G. N. Knyazheva,[1] I. M. Itkis,[1] M. G. Itkis,[1] K. V. Novikov,[1] D. Kumar,[1,2] T. Banerjee,[1] I. N. Diatlov,[1] M. Cheralu,[1] V. V. Kirakosyan,[1] Y. S. Mukhamejanov,[1,3,4] A. N. Pan,[1,3] I. V. Pchelintsev,[1] R. S. Tikhomirov,[1] I. V. Vorobiev,[1] M. Maiti,[5] R. Prajapat,[5] R. Kumar,[5] G. Sarkar,[5] W. H. Trzaska,[6] A. N. Andreyev,[7,8] I. M. Harca,[9,10] and E. Vardaci[11,12]

[1]*Flerov Laboratory of Nuclear Reactions, Joint Institute for Nuclear Research, 141980 Dubna, Russia*
[2]*GSI Helmholtzzentrum für Schwerionenforschung, 64291 Darmstadt, Germany*
[3]*Institute of Nuclear Physics, Almaty 050032 Kazakhstan*
[4]*Al-Farabi Kazakh National University, Almaty 050040 Kazakhstan*
[5]*Department of Physics, Indian Institute of Technology Roorkee, 247667 Uttarakhand, India*
[6]*Department of Physics, University of Jyväskylä, FIN-40014 Jyväskylä, Finland*
[7]*Department of Physics, University of York, York YO10 5DD, United Kingdom*
[8]*Advanced Science Research Center, Japan Atomic Energy Agency, Tokai, Ibaraki 319-1195, Japan*
[9]*Facility for Rare Isotope Beams, Michigan State University, East Lansing Michigan 48824, USA*
[10]*Horia Hulubei National Institute for R&D in Physics and Nuclear Engineering, Bucharest-Magurele, Romania*
[11]*Dipartimento di Fisica "E. Pancini," Universita degli Studi di Napoli "Federico II," 80126 Napoli, Italy*
[12]*Istituto Nazionale di Fisica Nucleare, Sezione di Napoli, 80126 Napoli, Italy*

(Received 27 June 2021; revised 26 July 2021; accepted 18 August 2021; published 31 August 2021)

Background: Observation of asymmetric fission of ^{180}Hg has led to intensive theoretical and experimental studies of fission of neutron-deficient nuclei in the lead region.
Purpose: The study of asymmetric and symmetric fission modes of ^{180,190}Hg and ^{184,192,202}Pb nuclei.
Methods: Mass-energy distributions of fission fragments of ^{180,190}Hg and ^{184}Pb formed in the ^{36}Ar + ^{144,154}Sm and ^{40}Ca + ^{144}Sm reactions, respectively, at energies near the Coulomb barrier have been measured using the double-arm time-of-flight spectrometer CORSET and compared with previously measured ^{192,202}Pb isotopes produced in the ^{48}Ca + ^{144,154}Sm reactions. The mass distributions for ^{180,190}Hg and ^{184,192,202}Pb together with old data for ^{187}Ir, ^{195}Au, ^{198}Hg, ^{201}Tl, ^{205,207}Bi, ^{210}Po, and ^{213}At [J. Nucl. Phys. **53**, 1225 (1991)] have been decomposed into symmetric and asymmetric fission modes. The total kinetic-energy distributions for different fission fragment mass regions have been analyzed for ^{180,190}Hg and ^{184}Pb.
Results: The stabilization role of proton numbers at $Z \approx 36$, 38, $Z \approx 45$, 46, and $Z = 28/50$ in asymmetric fission of excited preactinide nuclei has been observed. The high ($\approx$ 145-MeV) and the low ($\approx$ 128-MeV) energy components have been found in the total kinetic-energy distributions of ^{180,190}Hg fission fragments corresponding to the fragments with proton numbers near $Z \approx 46$ and $Z \approx 36$, respectively. In the case of fission of ^{184}Pb only the low-energy component ($\approx$135 MeV) for the fragments with masses corresponding to the proton numbers $Z \approx 36$ and 46 has been found.
Conclusions: The studied properties of asymmetric fission of ^{180,190}Hg and ^{184,192,202}Pb nuclei point out the existence of well deformed proton shell at $Z \approx 36$ and less deformed proton shell at $Z \approx 46$.

DOI: 10.1103/PhysRevC.104.024623

I. INTRODUCTION

Fission of atomic nuclei is a complex process of directed collective motion of nucleons characterized by a significant change in shape, rearrangement of the nucleon configurations, redistribution of the nucleus excitation energy between its various types (vibrational, thermal, etc.). To describe fission, Strutinsky proposed considering the potential energy of a fissionable nucleus as the sum of the liquid-drop (macroscopic) potential and the shell correction [1]. The shell correction, being an oscillating function of deformation [2,3], noticeably transforms the shape of the potential-energy surface.

For actinides, the macroscopic component of the potential energy of the fissionable nucleus is comparable with the shell correction (~5–7 MeV), which results in a strong influence of shell effects in their fission. To date, the spontaneous and low-energy fission of actinides has been fairly well studied. It was found that they divide mainly asymmetrically with a heavy fragment mass of 142–144 u due to the proton and neutron shells [4–6]. The contribution of the symmetric mode increases with increasing excitation energy and becomes dominant at excitation energy greater than 40–50 MeV.

In the case of preactinides ($Z < 89$), the liquid-drop part of the potential energy of the fissioning nucleus is

 ©2021 American Physical Society

significantly higher than the shell correction. Thus, the symmetric fission mode prevails. Until the end of the 1980s, all experimental data on preactinides were in good agreement with the liquid-drop model (LDM) calculations, assumed only one mass-symmetric fission valley [7,8]. Hence, the observation of asymmetric fission of ^{187}Ir, ^{195}Au, ^{198}Hg, ^{201}Tl, ^{205,207}Bi, ^{210}Po, and ^{213}At [9–11] was quite unexpected. The most pronounced asymmetric fission mode was found for nuclei with the fissility parameter $x \approx 0.7$. To describe the mass distributions, the transition-state method was elaborated with an empirical positive shell correction for the mass-symmetric fission valley. This approach allowed to estimate the value of the shell correction of about 1 MeV to the fission barriers of preactinides but did not answer the questions concerning, first, the nature of the shell corrections and, second, the proton and neutron numbers playing a role in shell effects and the formation of fission fragments.

The nuclei in the regions of Ra [12,13], Ac [14,15], and the light isotopes of Th [16–18] are transitional cases between symmetric and asymmetric modes of fission inherent to actinides. In this case the mass distributions are a superposition of symmetric and asymmetric modes with comparable contributions. The trace of asymmetric modes typical for fission of actinides have been observed starting from Po and At with a yield of about 0.1% [19].

Recently, in experiments on the β-delayed fission of ^{180}Tl [20], an asymmetric mass distribution of the fission fragments of its daughter nucleus ^{180}Hg with an excitation energy $E^* < 10.8$ MeV was found. Note that the formation of two fragments—semimagic ^{90}Zr ($N = 50$, $Z = 40$)—should be expected in the symmetric fission of this strongly neutron-deficient nucleus. However, the formation of a light fragment with a mass of 80 u and a heavy one of 100 u was found most likely for ^{180}Hg. The observation of the asymmetric fission of ^{180}Hg [20] has renewed interest in the study of the fission properties of nuclei lighter than lead both theoretically [21–28] and experimentally [29–36]. However, there is still no unambiguous approach to understanding the fission of preactinides.

This paper is aimed at studying the asymmetric and symmetric nuclear fission modes in the lead region in dependence on the excitation energy and the nucleon composition of fissioning nuclei. The mass and energy distributions of fission fragments of ^{180,190}Hg formed in the ^{36}Ar + ^{144,154}Sm reactions and ^{184}Pb produced in the ^{40}Ca + ^{144}Sm reaction were measured using the double-arm time-of-flight spectrometer CORSET [37]. The previously measured fission fragments mass-energy distributions for ^{192,202}Pb obtained in the ^{48}Ca + ^{144,154}Sm reactions [38] were also included in our analysis.

The mass distributions of the fission fragments of ^{180,190}Hg, ^{184,192,202}Pb, as well as ^{187}Ir, ^{195}Au, ^{198}Hg, ^{201}Tl, ^{205,207}Bi, ^{210}Po, and ^{213}At from Refs. [9–11] were analyzed in the framework of a multimodal approach, successfully applied to describe the fission of actinides [6,17,39]. A generalized analysis of the data performed in this paper, as well as data from Refs. [9–11], significantly expanded the studied region of nuclei and allowed us to determine more accurately the proton and neutron numbers that affect the asymmetric fission properties in the lead region. The properties of the studied reactions are given in Table I.

TABLE I. The reactions under study, $E_{\rm lab}$: bombarding energy in the laboratory system; $\langle l \rangle$: mean angular momentum of the compound nucleus (CN); $\nu_{\rm pre}$: prescission neutron multiplicity; $E_{\rm pre}$: energy of prescission neutrons; $B(\langle l \rangle)$: angular momentum depended fission barrier [40]; $E^*_{\rm CN}$ and $E^*_{\rm SP}$: excitation energies of the formed CN and fissioning nucleus at the saddle point.

Reaction	CN	$E_{\rm lab}$ MeV	$E^*_{\rm CN}$ MeV	$\nu_{\rm pre}$	$E_{\rm pre}$ MeV	$\langle l \rangle$ $\hbar$	$B(\langle l \rangle)$ MeV	$E^*_{\rm SP}$ MeV
^{36}Ar + ^{144}Sm	^{180}Hg	158	34.1	0	0	8	10.0	24.1
		181	52.5	0.85	12.0	31	7.1	33.4
^{36}Ar + ^{154}Sm	^{190}Hg	158	56.7	1.10	14.1	8	13.2	29.4
		181	75.3	2.22	29.5	36	9.3	36.5
^{40}Ca + ^{144}Sm	^{184}Pb	180	35.3	0	0	8	8.0	27.3
		190	43.1	0.29	4.1	17	7.3	31.7
^{48}Ca + ^{144}Sm	^{192}Pb	182	33.4	0	0	9	10.8	22.6
		188	37.9	0	0	9	10.8	27.1
		202	48.4	0.60	7.9	33	7.9	32.6
^{48}Ca + ^{154}Sm	^{202}Pb	173	41.2	0.17	1.9	9	17.7	21.6
		183	48.8	0.63	7.3	9	17.7	23.8
		194	57.2	1.13	13.4	31	15.1	28.7

II. EXPERIMENT

The measurements were performed using the U400 cyclotron at the Flerov Laboratory of Nuclear Reactions, Dubna, Russia. The 235-μg/cm^2 ^{144,154}Sm targets deposited on 30-μg/cm^2 carbon backings were irradiated with the 180- and 190-MeV ^{40}Ca and 158- and 181-MeV ^{36}Ar beams. The target backings faced the beam. The details of measurements for the reaction with ^{48}Ca ions are given in Ref. [38]. The energy resolution was ~1%. Beam intensities on targets were 1 to 2 pnA. The enrichment of the ^{144,154}Sm targets was 93.8% and 98.9%, respectively.

The binary reaction products were measured in coincidence by the double-arm time-of-flight spectrometer CORSET [37]. Each arm of the spectrometer consists of a compact start detector and a position-sensitive stop detector based on microchannel plates. The angular acceptance of the spectrometer arms in the reaction plane was $\pm 10^\circ$ and $\pm 19^\circ$. In these experiments, the main attention was focused on detecting symmetric fragments formed in the complete fusion reaction. Thereby, according to the kinematics of the symmetric reaction fragments, the spectrometer arms were positioned symmetrically with respect to the beam axes at the angles $\pm 60^\circ$ corresponding to 90° in the center-of-mass (c.m.) system. The position resolution of the stop detectors was 0.3°, and the time resolution was about 150 ps. The mass and energy resolutions of the CORSET setup were deduced from the full width at half maximum of the mass and energy spectra of elastic particles, respectively. The mass and total kinetic energy (TKE) resolution of the spectrometer under these conditions was ± 2 u and ± 6 MeV, respectively.

Data processing assumed standard two-body kinematics [37]. Primary masses, velocities, energies, and angles of

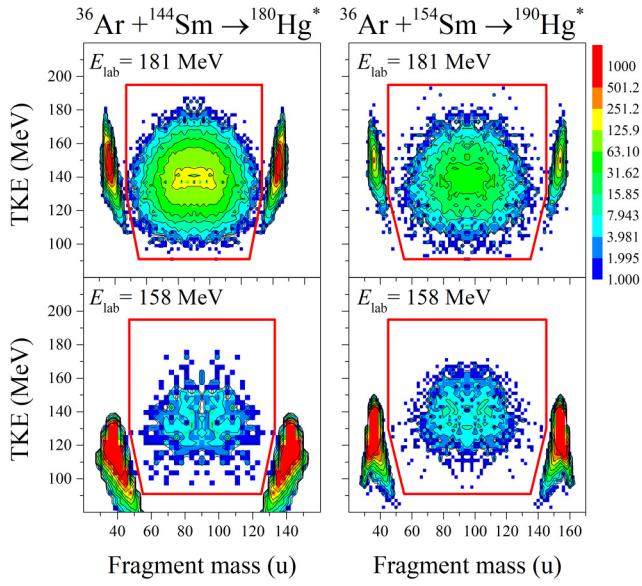

FIG. 1. The mass-energy distributions of binary fragments formed in the ^{36}Ar + ^{144,154}Sm reactions leading to the formation of mercury ($Z = 80$) isotopes at energies near the Coulomb barrier.

reaction products in the c.m. system were calculated from the measured velocities and angles using the momentum and mass conservation laws, assuming that the mass of the composite system is equal to $M_{\text{target}} + M_{\text{projectile}}$. Corrections for fragment energy losses in the target material and the foils of detectors were taken into account. The extraction of the binary reaction channels exhibiting full momentum transfer was based on the analysis of the kinematical diagram (see Refs. [37,41] for details).

III. RESULTS

Mass-total kinetic energy (M-TKE) distributions of the primary binary fragments obtained in the ^{36}Ar + ^{144,154}Sm, ^{40}Ca + ^{144}Sm, and ^{48}Ca + ^{144,154}Sm reactions leading to the formation of ^{180,190}Hg and ^{184,192,202}Pb isotopes at energies close to the Coulomb barrier are shown in Figs. 1 and 2. In the M-TKE distributions, the reaction products with masses close to those of the projectile and target and energies around $E_{\text{c.m.}}$ are associated with elastic and quasielastic events and can be separated well enough from other reaction channels. The fissionlike products located between the quasielastic peaks within the contour lines in the M-TKE distributions in Figs. 1 and 2 are characterized by large mass transfer and energy dissipation and can originate either from CN fission or QF processes.

A key parameter used to assess QF probability is the mean fissility parameter x_m [42]. It is expressed as $x_m = 0.75x_{\text{eff}} + 0.25x_{\text{CN}}$, where x_{CN} is a fissility of CN and x_{eff} is the effective fissility parameter [43] reflecting the entrance-channel mass and charge asymmetry. QF appears for reactions with $x_m > 0.68$ and results in widening of mass distributions and forward-backward asymmetry in angular distributions. The largest value of mean fissility parameter $x_m = 0.665$ is reached in the reaction ^{40}Ca + ^{144}Sm. This value is lower than the threshold value for QF appearance. So, all studied reactions are favorable for CN formation. For the ^{36}Ar + ^{144,154}Sm reactions, QF was not observed in the previous studies [29,33].

However, fusion suppression and the presence of asymmetric QF at energies near and below the Coulomb barrier have been observed for the reaction of ^{48}Ca with the deformed ^{154}Sm target [38]. In this case the asymmetric QF results in

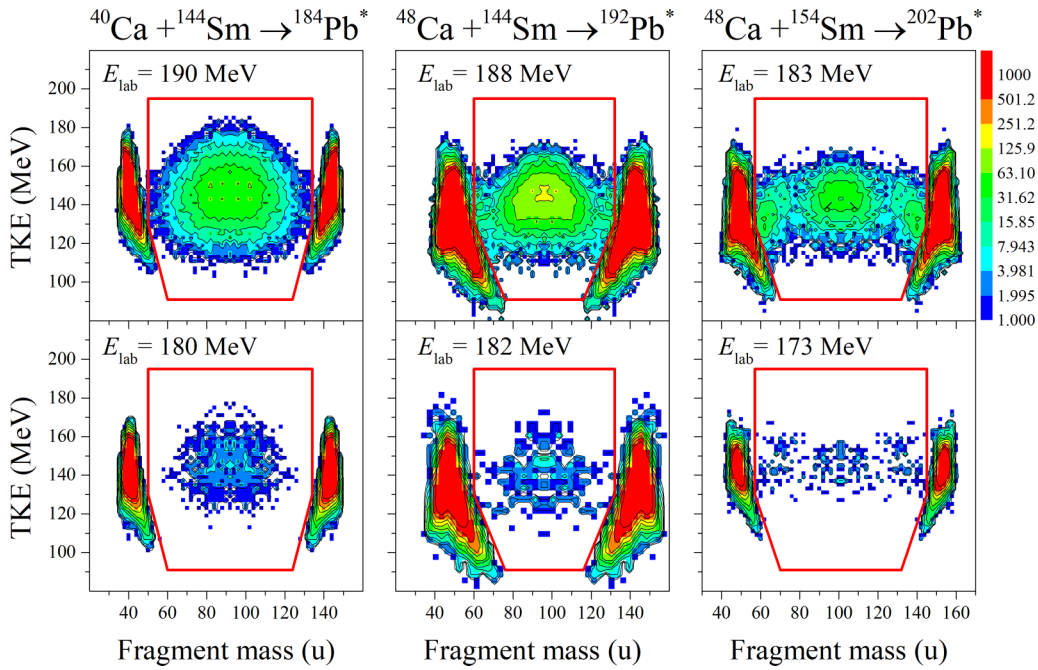

FIG. 2. The mass-energy distributions of binary fragments formed in the ^{40}Ca + ^{144}Sm and ^{48}Ca + ^{144,154}Sm reactions leading to the formation of lead ($Z = 82$) isotopes at energies near the Coulomb barrier.

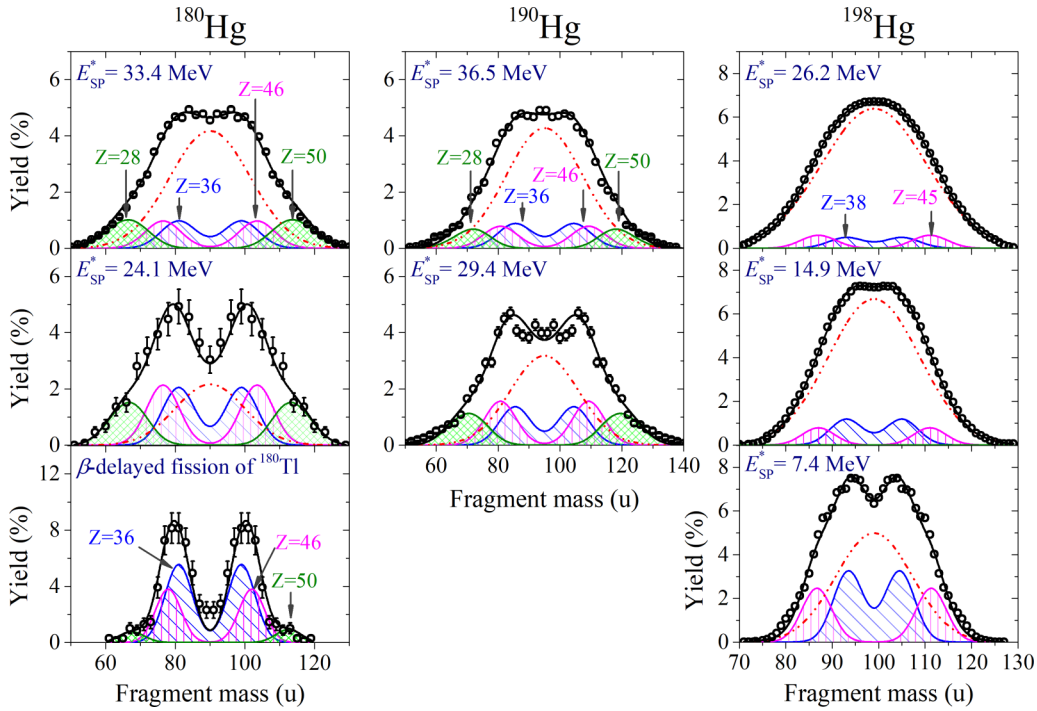

FIG. 3. Left and middle panels: the experimental mass distributions of fission fragments of ^{180,190}Hg, formed in the ^{36}Ar + ^{144,154}Sm reactions (open circles), left bottom panel: the experimental mass distribution of β-delayed fission of ^{180}Tl [20]; right panels: the mass distributions of the ^{198}Hg fission fragments [10] formed in the ^{197}Au (p, f) and ^{194}Pt (α, f) reactions. The lines correspond to the decompositions of mass distributions into the symmetric S (dashed-dot-dot lines), the asymmetric $A1$ (diagonally hatched region), the asymmetric $A2$ (vertically hatched region), and the asymmetric $A3$ (crosswise hatched region) modes.

the asymmetric fragments with masses of 60–75 u for the light fragment and 127–142 u for the heavy one. For more symmetric fragments, the signatures of QF presence have not been observed. For the ^{48}Ca + ^{144}Sm reaction with a spherical ^{144}Sm target, no evidence of QF has been found [38].

Therefore, we can expect that for all studied systems the fragments inside the contour lines in Figs. 1 and 2 originate from the CN-fission process, except for ^{48}Ca + ^{154}Sm. But even for this reaction, the fragments in the symmetric mass region 75–127 u are the products of the CN fission.

The excitation energies of formed CNs vary from 34 up to 75 MeV (see Table I). In this case the prescission neutron and proton emissions have to be taken into account. The prescission neutron multiplicities estimated using the systematics [44] are listed in Table I. The number of protons emitted before scission was estimated using NRV code [45]. For neutron-deficient ^{180}Hg and ^{184}Pb nuclei neutron evaporation is about three times more probable than proton one. For ^{192,202}Pb and ^{190}Hg the prescission proton emission is found to be less than 1%. We neglected proton evaporation in our paper. Therefore, the actual fissioning isotope may differ from the CN in terms of the neutron number, especially at the highest excitation energies.

IV. ANALYSIS AND DISCUSSION

A. Mass distributions of fission fragments

The mass distributions of fission fragments of excited ^{180,190}Hg and ^{184,192,202}Pb (events inside the contour lines in the M-TKE distributions in Figs. 1 and 2) normalized to 200% are presented in Figs. 3 and 4. The mass distributions of ^{198}Hg [10] formed in the reactions ^{197}Au (p, f) and ^{194}Pt (α, f) and β-delayed fission of ^{180}Tl [20] are also shown in Fig. 3 for comparison.

The investigations of fission fragment angular distributions [46] show that the preactinides have very large deformations in the transition states (saddle point). According to the calculations within the different versions of the LDM [47–49], a dumbbell-like shape with a thin neck close to the scission shape is proper to these large deformations of fissioning nuclei. Therefore, we may expect that the influence of dynamic effects on the descent from fission barrier to scission point is comparatively small, and the fragment formation is generally defined by the deformation potential-energy landscape in the vicinity of the saddle point. This is opposite to the fission of actinides characterized by a long descent from the saddle to scission in which the dynamical effects may strongly affect the fission process.

Thus, the fission properties of preactinide nuclei are mainly determined at the saddle point and depend on its excitation energy in the simplest approximation defined as

$$E^*_{\rm SP} = E^*_{\rm CN} - B_f(\langle l\rangle) - E_{\rm pre}, \qquad (1)$$

where $B_f(\langle l\rangle)$ is the angular momentum depended fission barrier and $E_{\rm pre}$ is the energy loss due to prescission neutron emission. Since the angular momenta introduced by the Ar and Ca projectiles are relatively large (see Table I), we used a fission barrier for the rotating liquid drop [40]. The

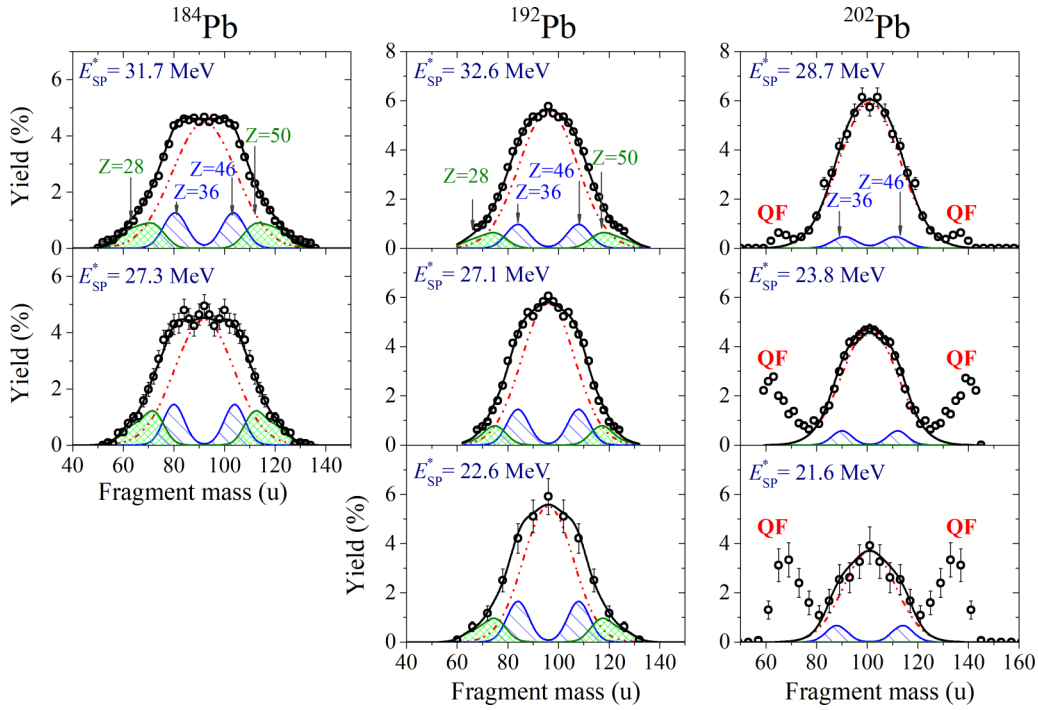

FIG. 4. The same as in Fig. 3 but for Pb isotopes formed in the ^{40}Ca + ^{144}Sm and ^{48}Ca + ^{144,154}Sm reactions.

ground-state shell corrections are less than 2.5 MeV for the studied nuclei [50]. Moreover, they decrease with increasing CN excitation energy [51], and we neglected them in the fission barrier calculation. In proton- and α-induced fission, the angular momentum introduced to the CN is negligibly small. The values of the interaction energies, excitation energies of formed CNs, mean angular momenta of the CN calculated with the PACE4 code [52], fission barriers at these momenta and excitation energies at the saddle point for the studied reactions are listed in Table I.

It is revealed from Fig. 3 that the mass distributions of fission of neutron-deficient nuclei ^{180,190}Hg have a pronounced asymmetric component even at rather high excitation energies. The positions of the maxima in mass distribution for ^{180}Hg are the same as observed in the low-energy fission of ^{180}Hg ($E^* < 10.8$ MeV) obtained as a daughter nucleus after β decay of ^{180}Tl [20]. For the nucleus ^{198}Hg located near the β-stability line, the fission has asymmetric mode at $E^*_{\rm SP} = 7.4$ MeV, nearly disappearing at $E^*_{\rm SP} = 26.2$ MeV, and the shape of mass distribution becomes close to a single Gaussian. For ^{184}Pb, the mass distributions are flattopped in the symmetric mass region, whereas for the more neutron-rich ^{192,202}Pb isotopes the mass distributions are close to a single Gaussian, although at $E^*_{\rm SP} < 30$ MeV the deviations from a single Gaussian shape are observed (see Fig. 4).

In the analysis of fission of excited nuclei from ^{176}Os to ^{206}Pb [29,33], the mass distributions were proposed to be a sum of two Gaussians centered at complementary fragment masses, and the symmetric fission mode was not considered. However, in the case of excited nuclei, the contribution of the symmetric mode, described by the LDM, which increases with increasing the excitation energy of fissioning nucleus, has to be taken into account. The analysis of fragment mass distributions of fission of ^{205,207,209}Bi at different excitation energies [34] showed that triple-Gaussian fits (a sum of symmetric and asymmetric modes) give a better agreement with experimental mass distributions than double-Gaussian fits (only one asymmetric mode).

Therefore, a question about the number of fission modes of preactinide nuclei arises. For instance, for actinides the four main fission modes were distinguished both theoretically and experimentally. According to the model of Brosa *et al.* [53], the modes are as follows: the superlong symmetric mode (*S*); the standard I (*S*1) mode caused by the influence of proton $Z = 50$ and neutron $N = 82$ shells; the standard II (*S*2) mode determined by deformed neutron shell with $N \approx 88$; the standard III (*S*3) superasymmetric mode caused by the influence of proton $Z = 28$ and neutron $N = 50$ shells; and the supershort mode (*SS*), which manifests itself only when both the light and the heavy fission fragments are close in their nucleon composition to the double magic tin with $A \approx 132$.

Based on the analysis of fragment mass yields from the fission of preactinides from ^{187}Ir to ^{213}At, located near the β-stability line, at low excitation energies at the saddle point ($E^*_{\rm SP} \approx 7$–13 MeV) [54], the existence of two strongly deformed neutron shells in the formed fragments with $N \approx 52$ and $N \approx 68$ was supposed. However, it is impossible to explain the asymmetric fission for neutron-deficient nuclei by these neutron numbers. For instance, in the present ppaper and in Ref. [20] for ^{180}Hg the maximum yields in mass distributions for the light and the heavy fragments are observed at 80 and 100 u. For ^{190}Hg the maxima were found at 83 and 107 u. The same values of the most probable fragment masses for the asymmetric fission of ^{180,190}Hg have been found in Ref. [29]. According to the simple assumption of the unchanged charge density of *N*/*Z* equilibration [55], the most

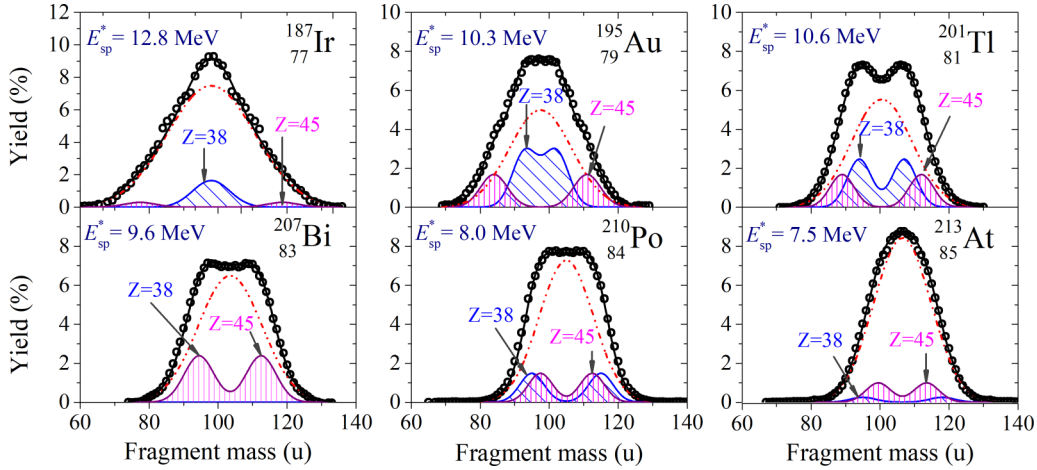

FIG. 5. The same as in Fig. 3 but for the ^{187}Ir, ^{195}Au, ^{201}Tl, ^{207}Bi, ^{210}Po, and ^{213}At nuclei obtained in the reactions with protons and α particles.

probable proton numbers of fragment pairs for both ^{180,190}Hg nuclei are $Z_L/Z_H \sim 35/45$, and the most probable neutron numbers are $N_L/N_H \sim 434/56$ for ^{180}Hg and $N_L/N_H \sim 48/62$ for ^{190}Hg. It suggests that in asymmetric fission of Hg isotopes, the proton numbers of fragments stay constant, whereas the neutron numbers change. Therefore, we may expect the existence of strongly deformed proton shells that affect the fission of preactinide nuclei and, thus, results in the formation of asymmetric fragments. For example, the calculation of Wilkins *et al.* [2] predicts well-deformed proton shells at $Z \approx 36$, 38, and 44.

It is to be noted that the detailed experimental study of low-energy fission of actinides [5,6] also revealed the stabilization role of proton numbers at $Z = 52$ for the $S1$ mode and $Z = 55$ for the $S2$ mode instead of $N = 82$ and 88 usually attributed to the $S1$ and $S2$ modes.

By analogy with actinides, we assume that the fission fragment mass distributions of the preactinide nuclei can be described as a sum of symmetric and several asymmetric modes, each asymmetric mode being a sum of two Gaussians centered at the complementary masses. The modes overlap, and, therefore, the variance of the symmetric mode should be fixed. Since we connect the symmetric mode with the macroscopic part of the potential energy to set its variance we use the empirical systematics based on the LDM [56].

The variance σ_M^2 increases linearly with $\langle l^2 \rangle$ and with the nuclear temperature T and can be written as [56]

$$\sigma_M^2 = \frac{\partial \sigma_M^2}{\partial T} T + \frac{\partial \sigma_M^2}{\partial \langle l^2 \rangle} \langle l^2 \rangle. \tag{2}$$

The first term in Eq. (2) corresponds to the variance of the mass distribution at zero angular momentum and can be calculated (with some assumptions) as

$$\sigma_M^2(l=0) = \frac{A_{CN}^2}{16} T \left[\left(\frac{d^2 V}{d\eta^2} \right)_{\eta=0} \right]^{-1}, \tag{3}$$

where A_{CN} is a mass number of the CN, $(d^2V/d\eta^2)_{\eta=0}$ is the stiffness of a nucleus at symmetric mass division ($\eta = 0$) and at zero angular momentum, which is derived from the corresponding systematics [56] for the temperature at the saddle point,

$$T = \sqrt{8.5 E^*_{SP}/A_{CN}}. \tag{4}$$

The sensitivity of the variance to the angular momentum is much weaker, although not negligible. To estimate the $\partial \sigma_M^2 / \partial \langle l^2 \rangle$ coefficient, we used similar systematics presented in Ref. [56].

The fission fragments mass distributions of nuclei from ^{187}Ir to ^{213}At can be described with one symmetric mode with Gaussian parameters given above, and two asymmetric modes associated with the proton shells at $Z \approx 38$ ($A1$ asymmetric mode) and $Z \approx 45$ ($A2$ asymmetric mode). These decompositions are shown in Fig. 5 for the lowest measured excitation energies ($E^*_{SP} < 13$ MeV). The widths of Gaussians corresponding to the asymmetric fission modes varied in the range of 3.5–5 u depending on the CN excitation energy. They are close to those found for the asymmetric mass distribution of ^{180}Hg from the β-delayed fission of ^{180}Tl (4 u). It is seen from Fig. 5 that the fragment mass distribution of fission of ^{187}Ir is symmetric, but it is not a Gaussian. Besides the LDM part, it contains a narrow symmetrical component. Similar mass distribution is observed in the case of spontaneous and low-energy fission of nuclei in the Fm–Rf region [57] (the so-called bimodal fission). It is important to note that bimodal fission appears for Fm isotopes ($Z = 100$) and heavier elements when both fragments are close to spherical proton ($Z = 50$) and/or neutron ($N = 82$) shells. For the ^{187}Ir ($Z = 77$), the number of protons in both fragments is close to $Z = 38$. Therefore, we may conclude that the proton number near $Z = 38$ plays an important role in the fission of nuclei in the sublead region. Besides, a small contribution of the $A2$ mode is needed to restore the mass distribution for ^{187}Ir more precisely. One can also see that asymmetric modes are more pronounced in the fission of Au, Tl, Bi, Po, and Hg, where both $A1$ and $A2$ modes have comparable intensities. The experimental data in Refs. [9–11] were measured at different

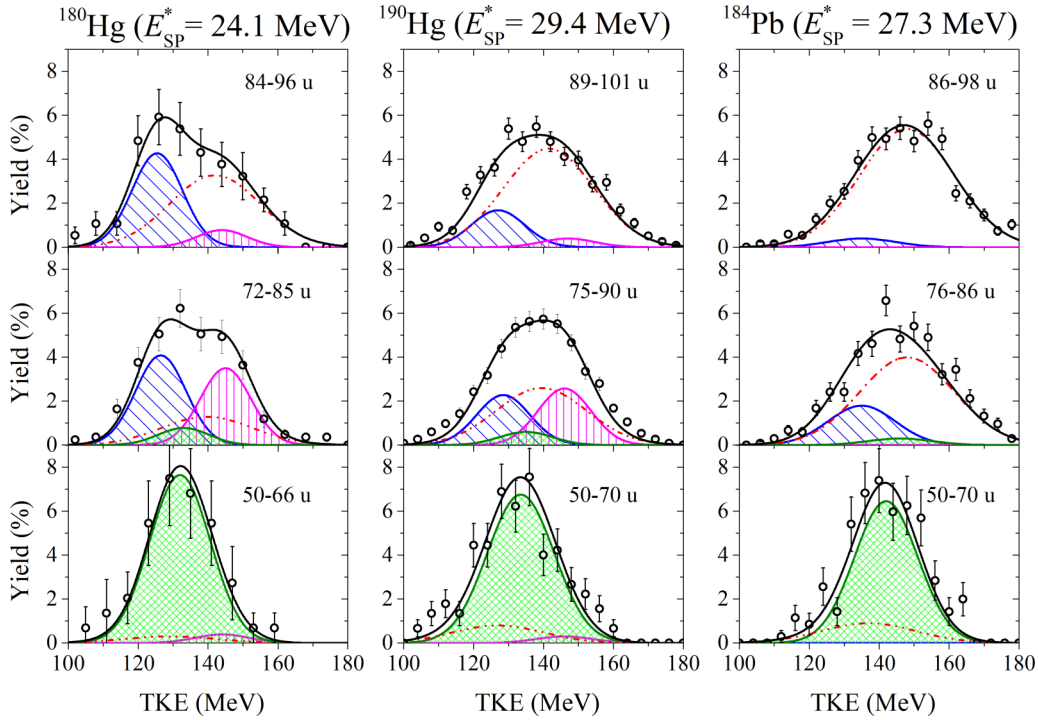

FIG. 6. TKE distributions of fragments for different mass regions for fission of ^{180,190}Hg and ^{184}Pb. The lines correspond to the decompositions of the TKE distributions into the symmetric (dashed-dot-dot lines), the asymmetric $A1$ (diagonally hatched region), the asymmetric $A2$ (vertically hatched region), and the asymmetric $A3$ (crosswise hatched region).

excitation energies of CNs. With increasing excitation energies, the shape of mass distribution becomes close to a single Gaussian with the parameters derived from the LDM at the saddle-point temperature $T_{SP} > 1.5$ MeV.

Mass distributions of neutron-deficient CNs of Hg and Pb isotopes also demand to involve one more asymmetric fission mode connected with the influence of $Z \approx 50$ and $Z \approx 28$ proton shells ($A3$ asymmetric mode) (see Figs. 3 and 4). This mode is observed in the excited fission of these nuclei as well as in the fission of ^{180}Hg at low excitation energy [20]. For the lead isotopes, the best fits of experimental data were found at $Z \approx 36$ for the $A1$ mode and at $Z \approx 46$ for the $A2$ mode. In this case the $A1$ mode is complementary to the $A2$ mode. As was mentioned above, the asymmetric fragments in the 60–75 u mass region for the light fragment and 127–142 u for the heavy one formed in the reaction ^{48}Ca + ^{154}Sm leading to the formation of ^{202}Pb are associated with the asymmetric QF process [38]. Therefore, it is impossible to distinguish the $A3$ mode in the fission of ^{202}Pb.

In Figs. 3–5 one can see that the modes S, $A1$, $A2$, and $A3$ overlap to a rather significant extent. Therefore, the description of the resulting mass distributions depends on the width of the Gaussian corresponding to the symmetric mode. Since the estimation of proton and neutron numbers of fission fragments is based on the unchanged charge density assumption, the prescission neutron evaporation may also add uncertainties to the obtained results of about 0.4 u. Moreover, the experimental resolution of our mass measurements is about ±2 u. For these reasons, we estimate the accuracy of proton numbers for the $A1$–$A3$ modes found at the fitting procedure of mass distributions as ±1 u, at least.

B. TKE distributions of fission fragments

The kinetic energy of fragments originates mainly from the Coulomb repulsion at the scission point. In the fission of actinides, the TKE values of the distinct modes were found to differ significantly [4]. The difference between the TKEs of the distinct modes can reach 20–25 MeV. We assume that in the fission of preactinides, the asymmetric modes can manifest themselves also in the TKE of fragments. In Fig. 6 the TKE distributions of fragments for different mass ranges for the fission of ^{180,190}Hg and ^{184}Pb at the lowest measured excitation energies are shown. The top panels show the TKE distributions for symmetric mass split, the middle panels—for the mass range where the yield of asymmetric fragments is maximal, the bottom panels—for the range where the $A3$ mode prevails according to the mass decompositions (see Figs. 3 and 4).

It is seen from Fig. 6 that the TKE distributions have a complex structure and change significantly with the fragments mass. We connect the S mode with the LDM valley. The most probable TKE value for this mode can be estimated using the Viola systematics [58]. According to the LDM, the TKE has a parabolic dependence on fragment mass,

$$\mathrm{TKE}(M) = 4\,\mathrm{TKE}_{\mathrm{Viola}}\frac{M(A_{\mathrm{CN}} - M)}{A_{\mathrm{CN}}^2}, \qquad (5)$$

where M is a fragment mass, $\mathrm{TKE}_{\mathrm{Viola}}$ is the most probable TKE.

In the case of ^{180}Hg, when the yield of the S mode is minimal compared to the ^{190,198}Hg (see Fig. 3), the TKE distribution for the symmetric mass split has a pronounced

TABLE II. The TKEs of the symmetric (S) and the asymmetric $A1$ ($Z \approx 36$), $A2$ ($Z \approx 46$), and $A3$ ($Z = 28/50$) fission modes for the studied reactions at the lowest measured energies.

		TKE (MeV)			
Reaction	CN	S	$A1$	$A2$	$A3$
^{36}Ar + ^{144}Sm	^{180}Hg	142 ± 2	127 ± 2	145 ± 2	132 ± 2
^{36}Ar + ^{154}Sm	^{190}Hg	142 ± 2	129 ± 2	146 ± 2	134 ± 2
^{40}Ca + ^{144}Sm	^{184}Pb	149 ± 2	135 ± 2	135 ± 2[a]	142 ± 2

[a]For this reaction the $A1$ and $A2$ modes are complementary to each other.

low-energy component (TKE ≈ 127 MeV). At the fitting procedure we did not fix the mean value for the S mode. The obtained values of mean TKE agree with the Viola ones within the error. This confirms our assumption of the LDM origin of this component. For fragment mass range of 72–85 u where the maximal contribution of asymmetric fission was found, both the low- (TKE ≈ 127-MeV) and the high-energy (TKE ≈ 145-MeV) components are observed. For the mass range of 50–66 u where the $A3$ mode prevails according to the decomposition shown in Fig. 3, we observed a main Gaussian with the TKE ≈ 132-MeV and minor contributions of other modes. Since the low-energy component appears for nearly symmetric fragments, we connect it with the $A1$ mode ($Z \approx 36$), whereas the high-energy component found for more asymmetric fragment masses—with the $A2$ mode ($Z \approx 46$). The experimental TKE distributions of fission of ^{180,190}Hg and ^{184}Pb for different mass ranges have been decomposed into the S, $A1$, $A2$, and $A3$ modes with the same weights as follows from the decompositions of mass distributions. These decompositions are also shown in Fig. 6. The deduced TKE values of the fission modes are listed in Table II.

The TKE of fragments depends on the distance d between the centers of the formed fragments at scission,

$$\mathrm{TKE[MeV]} = 1.44\frac{Z_1 Z_2}{d\mathrm{[fm]}}, \tag{6}$$

where Z_1 and Z_2 are the proton numbers of formed fragments. Thus, using the Eq. (6) we may estimate the elongation of the fissioning nucleus at the scission point for different modes. In the case of the fission of ^{180}Hg at $E^*_{\mathrm{SP}} = 23.9$ MeV the following values of distance have been found: for the S mode −16.2 fm, the $A1$ mode −18.0 fm, the $A2$ mode −15.5 fm, and the $A3$ mode −16.2 fm. Consequently, the shape at scission for the $A2$ mode is more compact than the LDM one, whereas for the $A1$ mode the shape is more elongated.

Recently it was found that the symmetric scission in the light thorium isotopes shows a compact configuration [18]. In this case, the number of protons is $Z = 45$ for both fragments that corresponds to the compact $A2$ mode proposed in our paper. Therefore, our results are consistent with the observed features of neutron-deficient Th nuclei, and the $A2$ mode may probably manifest itself in the fission of actinides.

In the fusion reaction ^{36}Ar + ^{154}Sm, leading to the formation of ^{190}Hg, the lowest measured energy of 158 MeV is close to the Coulomb barrier ($E_{\mathrm{c.m.}}/E_C = 0.98$) that corresponds to the CN excitation energy of 56.7 MeV. Unfortunately, the measurements of fission of ^{190}Hg at lower energies in this reaction are rather difficult due to the low counting rate. However, even at this relatively large excitation energy, the TKE distributions have a structure similar to the one observed for ^{180}Hg (see Fig. 6), whereas the contribution of the S mode is significantly higher. As it follows from Table II, the obtained values of mean TKE are similar to those that we found for ^{180}Hg for all fission modes.

Contrary to the fission of ^{180}Hg at similar excitation energy where the pronounced asymmetric component is observed, in the case of ^{184}Pb, the mass distribution for symmetric fragments is flattopped due to the dominance of symmetric mode. It is seen from Fig. 6 that the main parts of TKE distributions for the different mass ranges may be attributed with the S mode, described by the LDM. For symmetric mass range of 86–98 u, the low-energy component with TKE ≈ 135 MeV together with the S mode is observed. For fragment masses with maximal asymmetric yield (76–86 u), the yield of the low-energy component increases, whereas the high-energy component attributed to the $A2$ mode is not found. The absence of the high-energy component may be explained in a way that in the fission of Pb isotopes the $A1$ mode is complementary to the $A2$ mode (see the mass decomposition in Fig. 4). For the mass range of 50–70 u, the main component is the $A3$ mode with TKE ≈ 142 MeV.

Thus, the analysis of the TKE distributions of fission fragments for ^{180,190}Hg and ^{184}Pb confirms our assumption of the existence of several asymmetric modes in the fission of preactinide nuclei, namely, $A1$ and $A2$ connected with proton numbers $Z \approx 36$ and $Z \approx 46$, respectively, and the $A3$ mode caused by the proton shells at $Z = 28$ and/or $Z = 50$. The TKE values for these modes significantly differ.

C. Discussions and comparison with theory and other experimental data

The proton numbers of fission fragments, deduced in this paper for the $A1$ and $A2$ asymmetric modes, are shown as a function of the neutron numbers in Fig. 7. It is seen that for the $A1$ mode the proton numbers are close to $Z = 36$ for the fragments with less than 53 neutrons and about 38 for fragments with more than 53 neutrons. For the $A2$ mode $Z = 46$ for $N < 64$ and $Z = 45$ for $N > 64$.

As was mentioned above, according to the calculations of Wilkins *et al.* [2], the deformed proton shells at $Z \approx 38$ ($\beta_2 \approx 0.32$–0.42), $Z \approx 44$ ($\beta_2 \approx 0.50$–0.58), and $Z \approx 36$ ($\beta_2 \approx 0.67$–0.77) are expected. Recently, asymmetric fission has been studied theoretically in the sublead region using microscopic mean-field calculations of fission based on the Hartree-Fock approach [23]. Its origin is attributed to the influence of neutron shell gaps at $N = 52, 56$ for compact octupole deformations as well as shell gaps associated with large quadrupole deformations at $Z = 34$ and $Z = 42$–46 protons.

The analysis of experimental mass distributions of fission fragments of 14 nuclides between ^{176}Os and ^{206}Pb [33] with double-Gaussian fits shows that the deduced proton centroids are $Z = 36$–37 for the light fragments and 43–44 for the heavy ones. In the study of mass-asymmetric fission of ^{205,207,209}Bi [34], it was found that the light fragments have $Z \approx 38$ and $N \approx 56$–58 and the heavy fragments have $Z \approx 45$ and $N \approx$ 66-68.

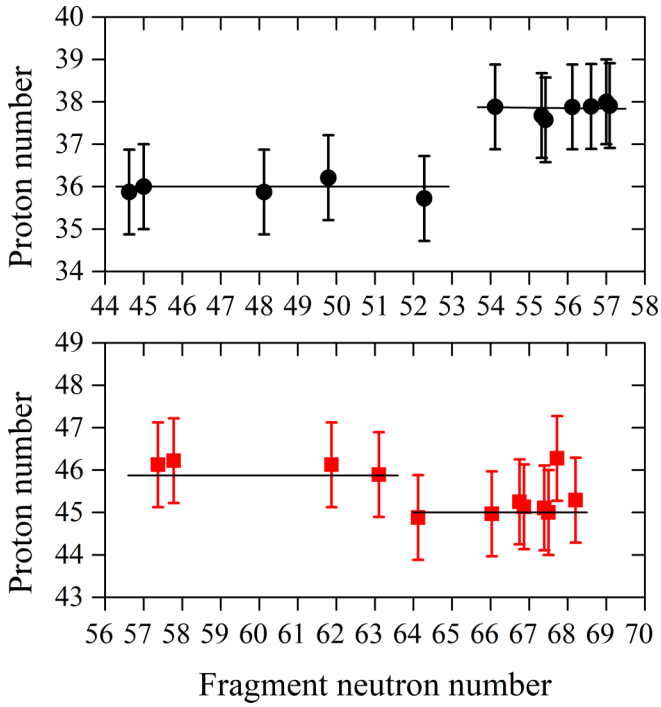

FIG. 7. The proton numbers for the $A1$ (top panel) and the $A2$ (bottom panel) modes in dependence on the neutron numbers of formed fragments.

Thus, the proton numbers obtained in this paper, which probably affect the asymmetric fission of preactinide nuclei, are close to those found in other experimental studies. The different theoretical approaches also predict similar proton numbers. In the present analysis, the stabilization role of neutron numbers at $N = 52, 68$ proposed in Ref. [54] and $N = 52, 56$ [23], which would be observed in the whole set of fission fragment mass distributions for nuclei from ^{187}Ir up to ^{213}At, has not been found.

The dependence of the ratio of the symmetric component contribution to the total yield of fission fragments for ^{180,190,198}Hg and ^{184,192,202}Pb on the excitation energy at the saddle point is shown in Fig. 8. The contributions of the symmetric mode are the smallest for fission of ^{180,190}Hg. For the lead isotopes, the yield of symmetric fission increases with increasing the neutron number of the fissioning nucleus. On the other hand, in the case of mercury nuclei, the yield of symmetric fission for ^{190}Hg is slightly lower than ^{180}Hg at the same excitation energies of CN at the saddle point. A similar trend for the fission of Hg isotopes has been predicted in Ref. [21], where it has been found that the fission of ^{188}Hg is more asymmetric than that of ^{180}Hg. In the case of ^{198}Hg and ^{202}Pb, located near the β-stability line, the fission is mainly symmetric at $E^*_{SP} > 20$ MeV.

V. SUMMARY

To investigate the dependence of the symmetric and asymmetric fission of preactinide nuclei on the excitation energy and neutron numbers of the CNs, the fission fragments mass-energy distributions of ^{180,190}Hg and ^{184}Pb formed in the

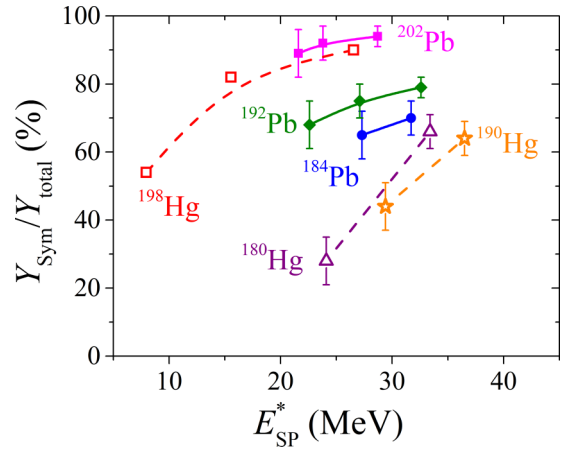

FIG. 8. The contribution of symmetric fission for ^{180,190,198}Hg and ^{184,192,202}Pb in dependence on excitation energy at the saddle point.

^{36}Ar + ^{144,154}Sm and ^{40}Ca + ^{144}Sm reactions were measured using the double-arm time-of-flight spectrometer CORSET. A generalized analysis of data obtained in this paper together with the data for ^{192,202}Pb nuclei, produced in the ^{48}Ca + ^{144,154}Sm reactions, measured previously with the CORSET setup, and the old data for ^{187}Ir, ^{195}Au, ^{198}Hg, ^{201}Tl, ^{205,207}Bi, ^{210}Po, and ^{213}At, significantly expanded the studied region and allowed us to determine the proton and neutron numbers that affect the asymmetric fission more accurately.

From the analysis of mass distributions for the whole set of the CN from ^{187}Ir up to ^{213}At, it was found that proton numbers at $Z \approx 36$, 38 and $Z \approx 45-46$ play a stabilization role in the asymmetric fission of these nuclei. In the case of ^{180,190}Hg and ^{184,192,202}Pb, the proton numbers are $Z \approx 36$ and 46. In the fission of lead isotopes, these proton numbers are complementary to each other. The fission fragments mass distributions of neutron-deficient Hg and Pb isotopes also demand to involve one more asymmetric mode connected with $Z = 50$ and $Z = 28$ proton shells. The stabilization role of neutron numbers appearing for all studied nuclei from ^{187}Ir up to ^{213}At in the present analysis was not revealed.

The analysis of the TKE distributions of ^{180,190}Hg and ^{184}Pb fission fragments confirm our assumption of the existence of several asymmetric modes. A high-energy component with TKE $\approx$ 145 MeV and a low-energy component with TKE $\approx$ 128 MeV, which correspond to the fragments with proton numbers close to $Z \approx 46$ and $Z \approx 36$, respectively, were found for the fission of ^{180,190}Hg. In the case of ^{184}Pb, only a low-energy component with TKE $\approx$ 135 MeV for the fragments around the proton numbers $Z \approx 36$ and 46 was found. For the fragments near the proton shells at $Z = 28$ and $Z = 50$, the TKE values are higher than associated with the LDM and amount to 133 MeV for ^{180,190}Hg and 142 MeV for ^{184}Pb. Thus, in the case of ^{180,190}Hg the shape of fissioning nuclei at the formation of fragment pairs with $Z = 34/46$ at scission point is more compact than the LDM one, whereas for the formation of fragment pair with $Z = 36/44$ (two protons shifted compared to $Z = 34/46$) the shape is more elongated.

In the case of lead isotopes, the yield of symmetric fission increases with increasing the neutron number of fissioning

nucleus. For ^{180,190}Hg the contributions of symmetric mode are lower than those for Pb isotopes. ^{198}Hg and ^{202}Pb, located near the β-stability line, undergoes mainly symmetric fission at the saddle point excitation energies higher than 20 MeV.

ACKNOWLEDGMENTS

We thank the FLNR accelerator team for excellent beam quality, smooth operation of the cyclotron throughout the experiment, and a friendly and professional attitude. Strong support of the directorate of the FLNR JINR is greatly acknowledged. This work was supported by the joint Grant from the Russian Foundation for Basic Research (Grant No. 19-52-45023) and the Department of Science and Technology of the Ministry of Science and Technology of India (Grant No. INT/RUS/RFBR/387). A.N.A. was supported by the Grant from STFC (United Kingdom).

[1] V. M. Strutinsky, Nucl. Phys. A **95**, 420 (1967).
[2] B. D. Wilkins, E. P. Steinberg, and R. R. Chasman, Phys. Rev. C **14**, 1832 (1976).
[3] I. Ragnarsson and R. K. Sheline, Phys. Scr. **29**, 385 (1984).
[4] F. Gonnenwein, *The Nuclear Fission Process* (CRC, Boca Raton, FL, 1991), Chap. 8, p. 287.
[5] K.-H. Schmidt, S. Steinhäuser, C. Böckstiegel, A. Grewe, A. Heinz, A. R. Junghans *et al.*, Nucl. Phys. A **665**, 221 (2000).
[6] C. Böckstiegel, S. Steinhäuser, K.-H. Schmidt, H.-G. Clerc, A. Grewe, A. Heinz, M. de Jong, A. R. Junghans, J. Müller, and B. Voss, Nucl. Phys. A **802**, 12 (2008).
[7] F. Plasil, D. S. Burnett, H. C. Britt, and S. G. Thompson, Phys. Rev. **142**, 696 (1966).
[8] A. W. Fairhall, Phys. Rev. **102**, 1335 (1956).
[9] M. G. Itkis, N. A. Kondratev, Yu. V. Kotlov, S. I. Mulgin, V. N. Okolovich, A. Y. Rusanov, and G. N. Smirenkin, Sov. J. Nucl. Phys. **47**, 4 (1988).
[10] M. G. Itkis, N. A. Kondratev, S. I. Mulgin, V. N. Okolovich, A. Y. Rusanov, and G. N. Smirenkin, Sov. J. Nucl. Phys. **52**, 601 (1990).
[11] M. G. Itkis, N. A. Kondratev, S. I. Mulgin, V. N. Okolovich, A. Y. Rusanov, and G. N. Smirenkin, Sov. J. Nucl. Phys. **53**, 757 (1991).
[12] H. C. Britt, H. E. Wegner, and J. C. Gursky, Phys. Rev. **129**, 2239 (1963).
[13] I. V. Pokrovsky, L. Calabretta, M. G. Itkis, N. A. Kondratiev, E. M. Kozulin, C. Maiolino, E. V. Prokhorova, A. Ya. Rusanov, and S. P. Tretyakova, Phys. Rev. C **60**, 041304(R) (1999).
[14] H. J. Specht, Nucleonika **20**, 717 (1975); Rev. Mod. Phys. **46**, 773 (1974).
[15] E. Konechy and H. W. Schmitt, Phys. Rev. **172**, 1213 (1968).
[16] K.-H. Schmidt, A. R. Junghans, J. Benlliure, C. Böckstiegel, H.-G. Clerc, A. Grewe *et al.*, Nucl. Phys. A **630**, 208 (1998).
[17] I. V. Pokrovsky, M. G. Itkis, J. M. Itkis, N. A. Kondratiev, E. M. Kozulin, E. V. Prokhorova *et al.*, Phys. Rev. C **62**, 014615 (2000).
[18] A. Chatillon, J. Taïeb, H. Alvarez-Pol, L. Audouin, Y. Ayyad, G. Belier *et al.*, Phys. Rev. Lett. **124**, 202502 (2020).
[19] M. G. Itkis, V. N. Okolovich, A. Y. Russanov, and G. N. Smirenkin, Z. Phys. A **320**, 433 (1985).
[20] A. N. Andreyev, J. Elseviers, M. Huyse, P. VanDuppen, S. Antalic, A. Barzakh *et al.*, Phys. Rev. Lett. **105**, 252502 (2010).
[21] P. Möller, J. Randrup, and A. J. Sierk, Phys. Rev. C **85**, 024306 (2012).
[22] T. Ichikawa, A. Iwamoto, P. Möller, and A. J. Sierk, Phys. Rev. C **86**, 024610 (2012).
[23] G. Scamps and C. Simenel, Phys. Rev. C **100**, 041602(R) (2019).
[24] J. D. McDonnell, W. Nazarewicz, J. A. Sheikh, A. Staszczak, and M. Warda, Phys. Rev. C **90**, 021302(R) (2014).
[25] A. V. Andreev, G. G. Adamian, and N. V. Antonenko, Phys. Rev. C **86**, 044315 (2012).
[26] A. V. Andreev, G. G. Adamian, N. V. Antonenko, and A. N. Andreyev, Phys. Rev. C **88**, 047604 (2013).
[27] H. Pasca, A. V. Andreev, G. G. Adamian, and N. V. Antonenko, Phys. Rev. C **101**, 064604 (2020).
[28] S. Panebianco, J.-L. Sida, H. Goutte, J.-F. Lemaître, N. Dubray, and S. Hilaire, Phys. Rev. C **86**, 064601 (2012).
[29] K. Nishio, A. N. Andreyev, R. Chapman, X. Derkx, C. E. Düllmann, L. Ghys *et al.*, Phys. Lett. B **748**, 89 (2015).
[30] E. Prasad, D. J. Hinde, K. Ramachandran, E. Williams, M. Dasgupta, I. P. Carter *et al.*, Phys. Rev. C **91**, 064605 (2015).
[31] R. Tripathi, S. Sodaye, K. Sudarshan, B. K. Nayak, A. Jhingan, P. K. Pujari *et al.*, Phys. Rev. C **92**, 024610 (2015).
[32] I. Tsekhanovich, A. N. Andreyev, K. Nishio, D. Denis-Petit, K. Hirose, H. Makii *et al.*, Phys. Lett. B **790**, 583 (2019).
[33] E. Prasad, D. J. Hinde, M. Dasgupta, D. Y. Jeung, A. C. Berriman, B. M. A. Swinton-Bland *et al.*, Phys. Lett. B **811**, 135941 (2020).
[34] B. M. A. Swinton-Bland, M. A. Stoyer, A. C. Berriman, D. J. Hinde, C. Simenel, J. Buete *et al.*, Phys. Rev. C **102**, 054611 (2020).
[35] C. Schmitt, A. Lemasson, K.-H. Schmidt, A. Jhingan, S. Biswas, Y. H. Kim *et al.*, Phys. Rev. Lett. **126**, 132502 (2021).
[36] E. M. Kozulin, E. Vardaci, W. H. Trzaska, A. A. Bogachev, I. M. Itkis, A. V. Karpov, G. N. Knyazheva, and K. V. Novikov, Phys. Lett. B **819**, 136442 (2021).
[37] E. M. Kozulin, A. A. Bogachev, M. G. Itkis, I. M. Itkis, G. N. Knyazheva, N. A. Kondratiev *et al.*, Instrum. Exp. Tech. **51**, 44 (2008).
[38] G. N. Knyazheva, E. M. Kozulin, R. N. Sagaidak, A. Y. Chizhov, M. G. Itkis, N. A. Kondratiev *et al.*, Phys. Rev. C **75**, 064602 (2007).
[39] S. I. Mulgin, S. V. Zhdanov, N. A. Kondratiev, K. V. Kovalchuk, and A. Y. Rusanov, Nucl. Phys. A **824**, 1 (2009).
[40] A. J. Sierk, Phys. Rev. C **33**, 2039 (1986).
[41] D. J. Hinde, M. Dasgupta, J. R. Leigh, J. C. Mein, C. R. Morton, J. O. Newton, and H. Timmers, Phys. Rev. C **53**, 1290 (1996).
[42] R. du Rietz, E. Williams, D. J. Hinde, M. Dasgupta, M. Evers, C. J. Lin, D. H. Luong, C. Simenel, and A. Wakhle, Phys. Rev. C **88**, 054618 (2013).
[43] R. Bass, Nucl. Phys. A **231**, 45 (1974).
[44] D. Hilscher and H. Rossner, Ann. Phys. **17**, 471 (1992).

[45] A. V. Karpov, A. S. Denikin, M. A. Naumenko, A. P. Alekseev, V. A. Rachkov, V. V. Samarin, V. V. Saiko, and V. I. Zagrebaev, Nucl. Instrum. Methods Phys. Res., Sect. A **859**, 112 (2017); http://nrv.jinr.ru/nrv.
[46] A. V. Ignatyuk, G. N. Smirenkin, M. G. ltkis, S. I. Mulgin, and V. N. Okolovich, Phys. Part. Nucl. **16**, 307 (1985).
[47] W. D. Myers and W. J. Swiatecki, Ark. Fys. **36**, 343 (1967).
[48] V. M. Strutinsky, Sov. J. Nucl. Phys. **1**, 588 (1965).
[49] H. J. Krappe, J. R. Nix, and A. J. Sierk, Phys. Rev. C **20**, 992 (1979).
[50] P. Möller, A. J. Sierk, T. Ichikawa, and H. Sagawa, At. Data Nucl. Data Tables **109–110**, 1 (2016).
[51] A. V. Ignatyuk, M. G. Itkis, V. N. Okolovich, G. N. Smirenkin, and A. S. Tishin, Sov. J. Nucl. Phys. **21**, 612 (1975); A. V. Ignatyuk, G. N. Smirenkin, and A. S. Tishin, *ibid.* **21**, 255 (1975).
[52] A. Gavron, Phys. Rev. C **21**, 230 (1980); O. B. Tarasov and D. Bazin, Nucl. Instrum. Methods Phys. Res., Sect. B **266**, 4657 (2008).
[53] U. Brosa, S. Grossmann, and A. Muller, Phys. Rep. **197**, 167 (1990).
[54] S. I. Mulgin, K.-H. Schmidt, A. Grewe, and S. V. Zhdanov, Nucl. Phys. A **640**, 375 (1998).
[55] R. Vandebosch and J. R. Huizenga, *Nuclear Fission* (Academic, New York, 1973).
[56] M. G. Itkis and A. Y. Rusanov, Phys. Part. Nucl. **29**, 160 (1998).
[57] E. K. Hulet, J. F. Wild, R. J. Dougan, R. W. Lougheed, J. H. Landrum, A. D. Dougan *et al.*, Phys. Rev. Lett. **56**, 313 (1986); Phys. Rev. C **40**, 770 (1989).
[58] V. E. Viola, K. Kwiatkowski, and M. Walker, Phys. Rev. C **31**, 1550 (1985).